Carbon Trends 21 (2025) 100559

Contents lists available at ScienceDirect

Carbon Trends

journal homepage: www.elsevier.com/locate/cartre

The impact of thermal stabilization temperature and duration on the pore structure of polyacrylonitrile-based carbon nanofibers

T. Fischer [a,b,*], M. Pagel [a], A. Kretzschmar [a], V. Selmert [a,b], S. Jovanovic [a], R. Rameker [a,c], H. Kungl [a], H. Tempel [a], R.-A. Eichel [a,b]

[a] Forschungszentrum Jülich GmbH, Institute of Energy Technology (IET-1) – Fundamental Electrochemistry, 52425 Jülich, Germany
[b] RWTH Aachen University, Institute of Physical Chemistry, 52056 Aachen, Germany
[c] RWTH Aachen University, Institute of Technical and Macromolecular Chemistry, 52056 Aachen, Germany

ARTICLE INFO

Keywords:
Gas adsorption
Ladder polymer
Pore formation
Structural properties
Ultramicropore
Carbon modification

ABSTRACT

This work analyzes the impact of temperature and duration during thermal stabilization of polyacrylonitrile-based (PAN-based) nanofibers on the pore formation of carbon nanofibers. Two sample series at different stabilization durations (0–15 h) and temperatures (200–300 °C) were synthesized and characterized by Fourier-transform infrared spectroscopy, Raman spectroscopy, elemental analysis, solid state nuclear magnetic resonance and gas adsorption. A significant increase of the pore volume of the carbonized nanofibers from 0.039 $cm^3\ g^{-1}$ to 0.171 $cm^3\ g^{-1}$ was obtained for long stabilization durations (> 4 h). Similar increases up to 0.166 $cm^3\ g^{-1}$ were obtained at high stabilization temperatures (> 250 °C). This increased pore formation was assigned to the growth of larger stabilized ladder polymers and a high incorporation of oxygen during the thermal stabilization at these conditions. Both alter the structure of the final carbon nanofibers and strongly affect the formation of pore volume during carbonization. Especially, the formation of the ultramicropore volume was found to be highly dependent on these parameters. The results show the necessity of a careful consideration of the thermal stabilization conditions for tailoring of the pore structure of PAN-based carbon nanofibers.

1. Introduction

Carbon nanofibers based on polyacrylonitrile (PAN) are applied in various fields, such as aerospace [1–4], automotive [5,6], supercapacitors [7,8] and gas adsorption processes [9–12].

Their synthesis commonly proceeds via the steps of electrospinning, thermal stabilization, carbonization and optional graphitization [13–15]. The electrospun PAN nanofibers undergo thermal stabilization in air or inert atmosphere at temperatures between 200–300 °C, resulting in the formation of the stabilized ladder polymer. The occurring chemical reactions during this step are a sequence of cyclization, dehydrogenation and oxidation reactions [16–20] (Fig. 1).

Subsequent to the stabilization, carbonization is conducted in inert atmosphere, i.e. N_2 or Ar, at temperatures higher than 400 °C [13]. During this step, the stabilized ladder polymer segments interconnect and a large carbon framework is formed [13]. Finally, graphitization can be applied at temperatures higher than 1600 °C [14].

Current investigations focus on the impact of the carbonization step on the gas adsorption properties and the underlying pore system of the carbon nanofibers [10,11,22–26]. For instance, remarkable CO_2/N_2 selectivity values and carbonization temperature dependent molecular sieve properties were found [10,24]. Moreover, a decrease of the cumulative pore volume from 0.172 $cm^3\ g^{-1}$ to 0.070 $cm^3\ g^{-1}$ at an increase of the carbonization temperature from 600 to 1100 °C was determined [23]. Thus, the carbonization conditions were found to decisively influence the developed pore structure.

Far less attention received the impact of the thermal stabilization on the pore structure and corresponding gas adsorption properties of carbon nanofibers. In recent works, a beneficial impact of an increased stabilization temperature and duration was reported, stating a 46 % increased CO_2 adsorption capacity by changing the stabilization conditions from 230 °C, 1 h to 260 °C, 2 h [27]. However, the study compares only two stabilization conditions and does vary two essential stabilization parameters simultaneously. Thus, it is challenging to assess the impact of each individual parameter.

A second publication reports a reduction of the CO_2 adsorption

* Corresponding author.
E-mail address: to.fischer@fz.juelich.de (T. Fischer).

https://doi.org/10.1016/j.cartre.2025.100559
Received 4 February 2025; Received in revised form 7 August 2025; Accepted 7 August 2025
Available online 8 August 2025

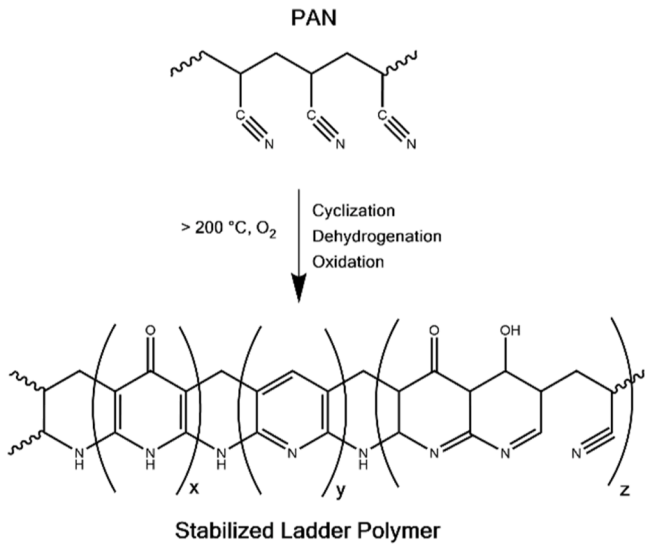

Fig. 1. Simplified scheme of the cyclization of polyacrylonitrile during thermal stabilization resulting in the formation of the stabilized ladder polymer [21].

capacities at increasing stabilization temperatures from 250 to 300 °C [28] which is an opposing trend compared to the first publication. Since both studies cover only parts of the commonly applied stabilization temperature range, a holistic view on the impact of stabilization temperature on the CO_2 adsorption capacities is currently missing.

Moreover, the evaluation of the impact of thermal stabilization on the pore structure after carbonization is currently limited to the calculation of preferential pore diameters [28], whereas the pore size distribution is not discussed.

Thus, the present work aims to improve the current data to provide a better understanding of the impact of the stabilization duration and temperature on the pore structure of carbonized nanofibers.

Carbon nanofibers stabilized at different durations from 0 to 15 h at 250 °C and different temperatures from 200 to 300 °C for 1 h in air are synthesized and investigated by gas adsorption focussing on the pore structure using quenched solid density functional theory (QSDFT) and Monte-Carlo calculation models to analyze the pore size distribution [29,30].

Additional analytical techniques, such as Fourier transform infrared spectroscopy (FT-IR), elemental analysis, ^{13}C magic angle spinning nuclear magnetic resonance (^{13}C MAS-NMR), Raman spectroscopy and elemental analysis are applied to relate the chemical changes during the stabilization process to changes in pore structure of the carbonized nanofibers and identify essential factors.

2. Experimental

2.1. Synthesis

Custom-made electrospun PAN nanofibers (Stellenbosch Nanofiber Company, South Africa) were used as received. Scanning electron microscopy images of the nanofibers are attached in Figure S1.

Thermal stabilization was conducted in a ventilated drying cabinet (Carbolite Gero GmbH & Co. KG., Germany). The duration was varied between 0, 0.5, 1, 4, 8 and 15 h at a constant temperature of 250 °C. For investigation of the temperature impact, the stabilization temperature was set to 200, 225, 250, 275 and 300 °C for a duration of 1 h. All experiments were carried out in air and heating to the target temperature was conducted at a rate of 5 K min^{-1}. After stabilization, all samples were carbonized at 800 °C for 3 h in Ar (5.0, Air Products, France) using a heating rate of 5 K min^{-1} in a tubular furnace (Carbolite Gero GmbH & Co. KG., Germany).

2.2. Characterization

Attenuated total reflection (ATR) FT-IR spectroscopy measurements were conducted on a Spectrum 3 (PerkinElmer, USA) using a Diamond/ZnSe composite crystal. All measurements were performed at 32 scans at a resolution of 4 cm^{-1}. All spectra were baseline corrected. The peak height of the valence vibration of the C≡N ($\nu_{C\equiv N}$) and the *C=N/C=C* bonds ($\nu_{C=N/CC}$) was determined to calculate the cyclization index *CI* using Eq. (1). Based on the work of Collins et al. the absorptivity factor n was set to 0.29 [31,32].

$$CI = \frac{n \cdot \nu_{C=N/\ C=C}}{n \cdot \nu_{C=N/C=C} + \nu_{C\equiv N}} \cdot 100 \quad (1)$$

All IR investigations were conducted on the stabilized samples prior to the carbonization process.

Elemental analysis was performed on a VarioELcube elemental analyser (Elementar, Germany). A triple determination of C, H, N fractions and a single determination of the O fraction was conducted. Elemental analysis was performed for stabilized and carbonized samples.

Raman spectroscopy was conducted on the carbonized nanofibers using an Alpha R Raman microscope (WITec, Germany) at a laser wavelength of 532 nm and a laser power of 2 mW. A fivefold determination at different surface locations was conducted and the averaged spectrum was used for further analysis. The D and G band region of the obtained spectra was fitted using 5 Gaussian fits. The G band at 1570–1590 cm^{-1} was fitted using one Gaussian fit. Additionally, the D band was fitted using 4 Gaussian fits for D_1, D_2, D_3 and D_4 peaks which are related to defects and impurities of the carbon nanofibers [33–35]. The area of each fit was determined by integration and used for calculation of the D_1/G ratio.

Direct polarization ^{13}C NMR spectra were acquired using a Bruker Avance III HD spectrometer with a 14.1 T magnet and a 3.2 mm triple resonance MAS probe (PH MASDVT 600 W2 BL3.2 X/Y/H) at a spinning frequency of 20 kHz. As the NMR experiments were conducted using PAN samples with natural ^{13}C abundance, experiment time for quantitative spectra was optimized by utilizing 30 ° pulses (1.13 µs at 80 W) and a recovery delay of 25 s. For the sample stabilized for 15 h at 250 °C in air 16,384 scans and for the sample stabilized for 1 h at 200 °C 12,228 scans were used. All acquired ^{13}C spectra were externally referenced to adamantane. All NMR measurements were conducted on stabilized samples prior to carbonization.

The ^{13}C spectra were post-processed applying a 200 Hz line broadening. The peak fitting of the spectrum of sample stabilized for 15 h at 250 °C was performed using LMFIT version 1.3.3 [36] for Python 3.13 (64 bit), utilizing a non-linear least-squares algorithm. The signals were fitted using three Lorentz peak profiles for the aromatic compounds at 115.1, 136.9 and 154.5 ppm, two pseudo-Voigt peak profiles for the carbonyl compounds at 164.9 and 177.6 ppm and a Gauss peak profile for the signal at 28.2 ppm.

Gas adsorption measurements were conducted on a Micro 300 (3P Instruments, Germany) using CO_2 (4.5, Air Products, France) at 273 K and Ar (6.0, Air Products, France) at 87 K. Prior to each measurement, the samples were degassed for 12 h at 150 °C. Using Asiqwin 5.0 (Quantachrome Instruments, USA), the pore size distributions were calculated by Monte-Carlo calculations using a kernel for CO_2 at 273 K for slit pores on carbon. For the determination of the pore size distributions based on the Ar isotherms, a quenched solid state density functional theory (QSDFT) model with a kernel for slit pores on carbon was used. All Ar and CO_2 measurements were conducted on carbonized nanofibers.

The H_2O adsorption isotherms were measured on stabilized nanofibers prior to carbonization using a gravimetric vapor sorption analyzer in dynamic mode at a temperature of 298 K (DVS Vacuum, Surface Measurement Systems, United Kingdom). Prior to the measurement the samples were outgassed at 70 °C for 4 h.

3. Results and discussion

3.1. Impact of the stabilization duration (0–15 h)

A series of PAN nanofiber sheets was stabilized at durations of 0, 0.5, 1, 4, 8 and 15 h at 250 °C in air. After stabilization the white PAN nanofibers showed a distinct color change to dark brown, respectively black (*Figure S2*). The samples stabilized for short durations of 0.5 to 1 h were dark brown, whereas for stabilization times > 4 h a black color was obtained. This color change during stabilization was assigned to the formation of a large conjugated π-network in the stabilized ladder polymer [37].

3.1.1. Characterization

In-depth characterization of the ongoing chemical changes was conducted by FT-IR spectroscopy. To ensure comparability, the spectra were normalized to the height of the nitrile peak of the non-stabilized nanofibers (0 h) sample (Fig. 2a). For better visibility of the individual absorption bands, please refer to the spectra without normalization in the supporting information (Figure S3a).

The non-stabilized PAN nanofibers (0 h) spectrum shows four distinct absorption bands. At 2931 cm^{-1} CH_2 valence vibrations (ν_{CH2}) are observed which are assigned to the backbone CH_2 groups of PAN.

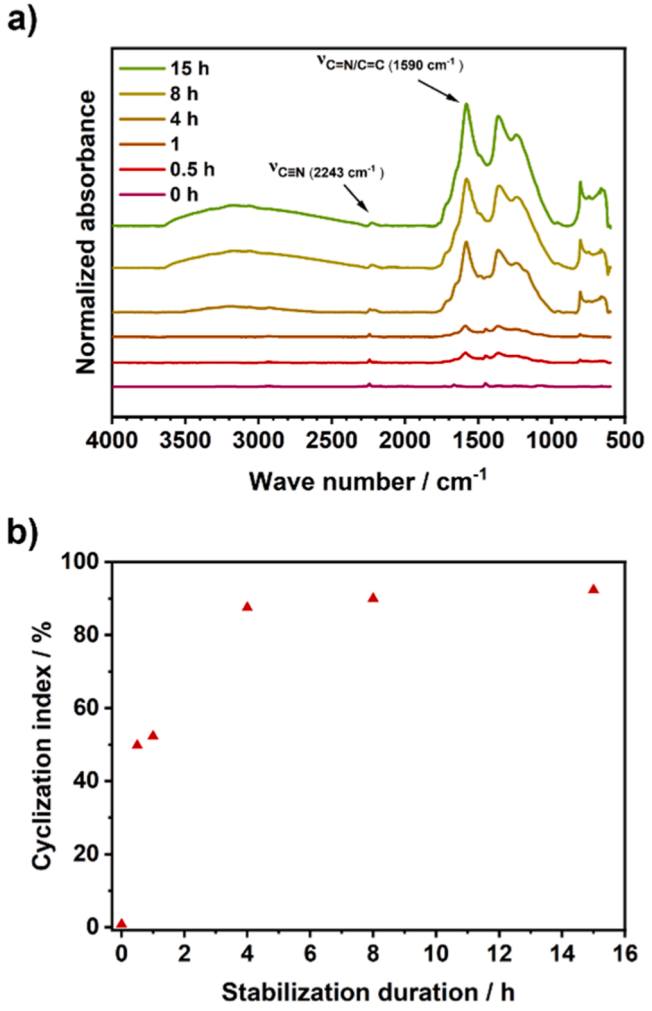

Fig. 2. (a) IR Spectra of PAN-based nanofibers thermally stabilized at 250 °C in air for durations of 0, 0.5, 1, 4, 8 and 15 h normalized to the nitrile absorption band of the non-stabilized sample (0 h). Non-normalized spectra can be found in S3. (b) Cyclization index determined based on the changes of the adsorption band heights of the 2243 cm^{-1} and 1590 cm^{-1} absorption band using Eq. (1).

Additionally, deformation vibrations of these groups (δ_{CH2}) are visible at 1454 cm^{-1}. The sharp absorption band at 2243 cm^{-1} is caused by the valence vibration of the nitrile groups ($\nu_{C\equiv N}$). The fourth absorption band at 1662 cm^{-1} is related to carbonyl valence vibrations ($\nu_{C=O}$), which are not directly related to PAN, but can be assigned to additives or impurities of the precursor.

At increasing stabilization duration, a significant decrease of $\nu_{C\equiv N}$ as well as a vanishing ν_{CH2} is observed. Simultaneously, new absorption bands at 1590 cm^{-1}, 1334 cm^{-1}, 1240 cm^{-1} and 801 cm^{-1} arise. The vibrations at 1590 cm^{-1} are assigned to -*C*=*N*- and -*C*=*C*- valence vibrations ($\nu_{C=N/C=C}$) of the stabilized ladder polymer, whereas the vibrations at 1334 cm^{-1} are deformation vibrations of CH groups (δ_{CH}) in the cyclized structure [38–40]. The absorption at 1240 cm^{-1} is most likely related to oxygen containing functional groups, e.g. carbonyl or hydroxyl groups. Additionally, the signal at 801 cm^{-1} is assigned to out-of-plane vibrations of the aromatic hydrogen atoms δ_{oop} [40].

Furthermore, a broad absorption band between 2300 and 3700 cm^{-1} arises in the spectra of the stabilized nanofibers at durations ≥ 4 h. This is assigned to ν_{O-H} of adsorbed water. The H_2O adsorption on the stabilized nanofibers prior to carbonization was investigated in vapor sorption experiments (Figure S4). An increase of the H_2O adsorption with prolonged stabilization duration was observed which is assigned to the higher polarity of these stabilized nanofibers. This is caused by an increased number of polar surface groups due to oxygen incorporation during the stabilization treatment.

After a stabilization duration of 4 h, $\nu_{C\equiv N}$ almost disappeared, whereas $\nu_{C=N/C=C}$ increased steadily which indicates a high progress of the cyclization reactions. To assess the progress of stabilization, the cyclization index based on the peak height of the $\nu_{C\equiv N}$ at 2243 cm^{-1} and $\nu_{C=C/C=N}$ at 1590 cm^{-1} was calculated (Eq. (1)). Within the first hour of stabilization, a steep rise to 52 % is obtained which further increases up to 87 % for 4 h stabilization duration (Fig. 2b). At longer stabilization durations only a small additional rise of the cyclization index to a maximum of 92 % is determined. These calculated cyclization indices match well with the qualitatively discussed changes in the FT-IR spectra.

Additionally, elemental analysis was conducted to determine changes in the elemental composition for all samples after stabilization and after carbonization (Fig. 3a,b).

After stabilization, a reduction of the C fraction from 65.6 to 52.5 wt.-% with increasing stabilization duration is observed. This decrease is mainly caused by the incorporation of oxygen into the stabilized ladder structure due to oxidation reactions. The incorporation of oxygen is clearly visible in the continuous increase of the oxygen fraction from 2.8 to 24.3 wt.- % which approaches a limiting value at stabilization durations > 4 h.

Simultaneously, a decrease of the N fraction from 26.0 to 19.9 wt.-% is observed. This is most likely only a relative decrease caused by the oxygen incorporation, since no significant nitrogen elimination during thermal stabilization is expected [41]. The reduction of the H fraction from 6.0 to 3.1 wt.-% indicates ongoing dehydrogenation reactions. However, the H fraction is also affected by the parallelly occurring reactions and therefore cannot be seen as a reliable measure for the dehydrogenation reactions.

After carbonization, the differences in elemental composition between the samples are diminished compared to the samples which were only stabilized. In particular, the removal of heteroatoms is observed. This reduction in heteroatom content is evident in the decreased oxygen fraction after the carbonization (Fig. 3b). In contrast to the measurements performed after stabilization, the oxygen fraction increases just from 8.3 to 11.6 wt.-% with increasing stabilization duration. The oxygen:carbon ratio decreased about 60 % for carbonized samples, which were stabilized ≥ 4 h, compared to after stabilization (Fig. 3c). The removal of oxygen during carbonization could occur via condensation reactions between adjacent stabilized ladder polymers [41]. The increase of the oxygen:carbon ratio for carbonized samples, which were stabilized for < 4 h, compared to the oxygen:carbon ratio after

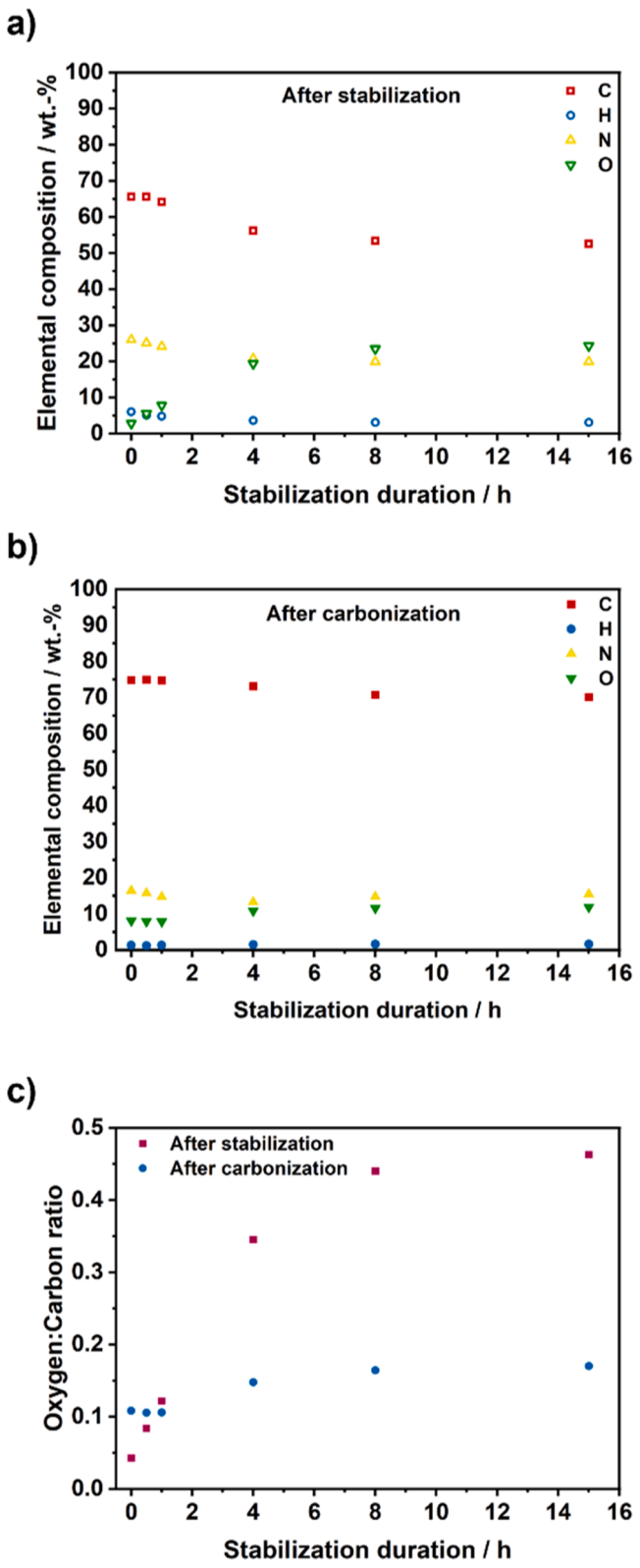

Fig. 3. (a) C, H, N, O elemental analysis of stabilized nanofibers synthesized at durations of 0, 0.5, 1, 4, 8 and 15 h at 250 °C in air. (b) C, H, N, O elemental analysis for carbonized nanofibers made from the nanofibers shown in (a). All carbonizations were conducted at 800 °C in Ar for 3 h. (c) Oxyen:carbon ratio for the nanofibers after stabilization and after carbonization.

stabilization is caused by the small degree of oxygen incorporated during stabilization. Thus, the removal of carbon surpasses the removal of oxygen during carbonization.

Similar to the oxygen fraction, a slight reduction of the H and N fractions is obtained after carbonization. This is expected due to N elimination and dehydrogenation reactions during carbonization. Within the sample series, only a slight decrease with longer stabilization durations is visible.

Due to the removal of heteroatoms during carbonization, the carbon fraction increases by 10 to 18 wt.- % compared to the stabilized nanofibers. The resulting carbon fraction is at 74.7 wt.-% for the non-stabilized carbon nanofibers and decreases slightly to 70.0 wt.-% after 15 h stabilization duration.

Due to the higher stabilization progress at long durations, larger stabilized ladder polymers are expected. These and additional cross-linking reactions via condensation due to the increased oxygen content could result in the growth of larger carbon frameworks during the carbonization step.

Such larger carbon frameworks would result in a higher degree of structural order in the carbon nanofibers. To assess the degree of structural order, the D_1/G ratio of the carbon nanofibers was determined by Raman spectroscopy (Fig. 4). The characteristic G band of a carbon material at ≈1580 cm^{-1} is related to the E_{2g} vibrations of the graphite

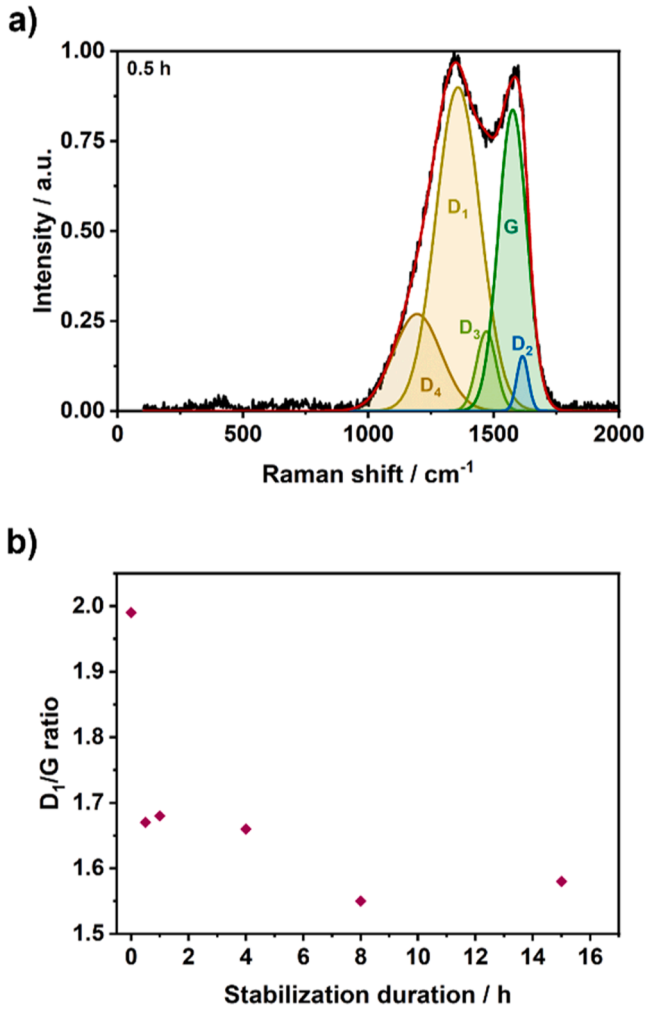

Fig. 4. (a) Raman D and G Band region for carbon nanofibers stabilized for 0.5 h at 250 °C in air. Spectrum measured after carbonization at 800 °C for 3 h in Ar. (b) D_1/G ratio determined based on the integration of the D and G band region of the carbon nanofibers stabilized at 0–15 h duration. All measurements were conducted on carbonized samples.

crystal lattice, whereas the D band at ≈1360 cm^{-1} is related to defects and disorder in the amorphous regions [33,42]. Five Gaussian fits were used to deconvolute the D and G region of the carbon nanofibers. One Gaussian fit was used for the G band and four fits (D_1, D_2, D_3 and D_4) are assigned to various defect types in the carbon structure (Fig. 4a, S5) [33, 43]. The D_1 band is assigned to disordered lattice vibrations with A_{1g} symmetry [44]. The D_2 band is commonly attributed to the disorder-induced phonon mode caused by defect structures [44] and the two additional fits D_3 and D_4 are frequently assigned to amorphous carbon regions including remaining heteroatoms (N, O) after carbonization [43,45,46]. Without stabilization, the D_1/G ratio is at 1.99. After 0.5 h stabilization, a steep decrease to 1.67 is observed, reflecting an increased structural order of the carbon nanofibers.

The decrease of the D_1/G ratio continuous at an attenuated course to a value of 1.58 after 15 h stabilization duration (Fig. 4b). Considering the results of the IR and elemental analysis, this increased structural order of carbon nanofibers stabilized for long durations can be related to the growth of larger stabilized ladder structures during thermal stabilization. The formation of larger stabilized structures, indicated by the increased cyclization index, results in larger carbon frameworks after carbonization. In addition to the increased size of the stabilized ladder structures, the increased incorporation of oxygen during stabilization could result in additional crosslinking reactions through the condensation of carbonyl groups, accompanied by the elimination of H_2O during carbonization [19,41]. The formation of carbonyl moieties during the thermal stabilization was verified using ^{13}C-solid-state NMR (See Section 3.2.1). Both, the larger stabilized ladder structures and the additional crosslinks would impact the developed carbon framework and thus influence the structural order of the carbon nanofibers.

3.1.2. *Impact on the pore structure*

To analyze the impact of the stabilization duration on the pore formation of the carbon nanofibers, Ar and CO_2 adsorption isotherms were recorded and evaluated. All isotherm measurements were conducted on carbonized samples.

For all samples, the Ar adsorption isotherms show a type II shape with <0.5 mmol g^{-1} Ar capacity (Fig. 5a). These isotherms are typical for non-porous adsorbents or adsorbents with pores inaccessible for the used adsorptive [47]. No trends between the stabilization duration and the Ar adsorption isotherms of the samples are observed. Based on the Ar isotherms, the BET area was determined which is between 3 and 7 m^2 g^{-1} on all samples (Table 1). Additionally, the isotherm data was used to calculate the pore size distribution by QSDFT calculations using a kernel for slit pores on carbon (Table 1, Figure S6a). Negligible cumulative pore volumes of <0.011 cm^3 g^{-1} were obtained. Both, BET area and pore size distribution, match the expectations well based on the isotherm shape.

To assess the supermicropore and ultramicropore volume (V_{Ultra}) of the carbon nanofibers, CO_2 adsorption isotherms at 273 K were measured. For non-stabilized carbon nanofibers (0 h) the isotherm shows an almost linear course with a negligible CO_2 uptake at relative pressures < 0.01 (Fig. 5b). At higher relative pressures, the capacity increases to 0.37 mmol g^{-1}. With longer stabilization durations the shape of the CO_2 adsorption isotherm changes significantly. Already after 0.5 and 1 h stabilization duration, the isotherm slope in the low-

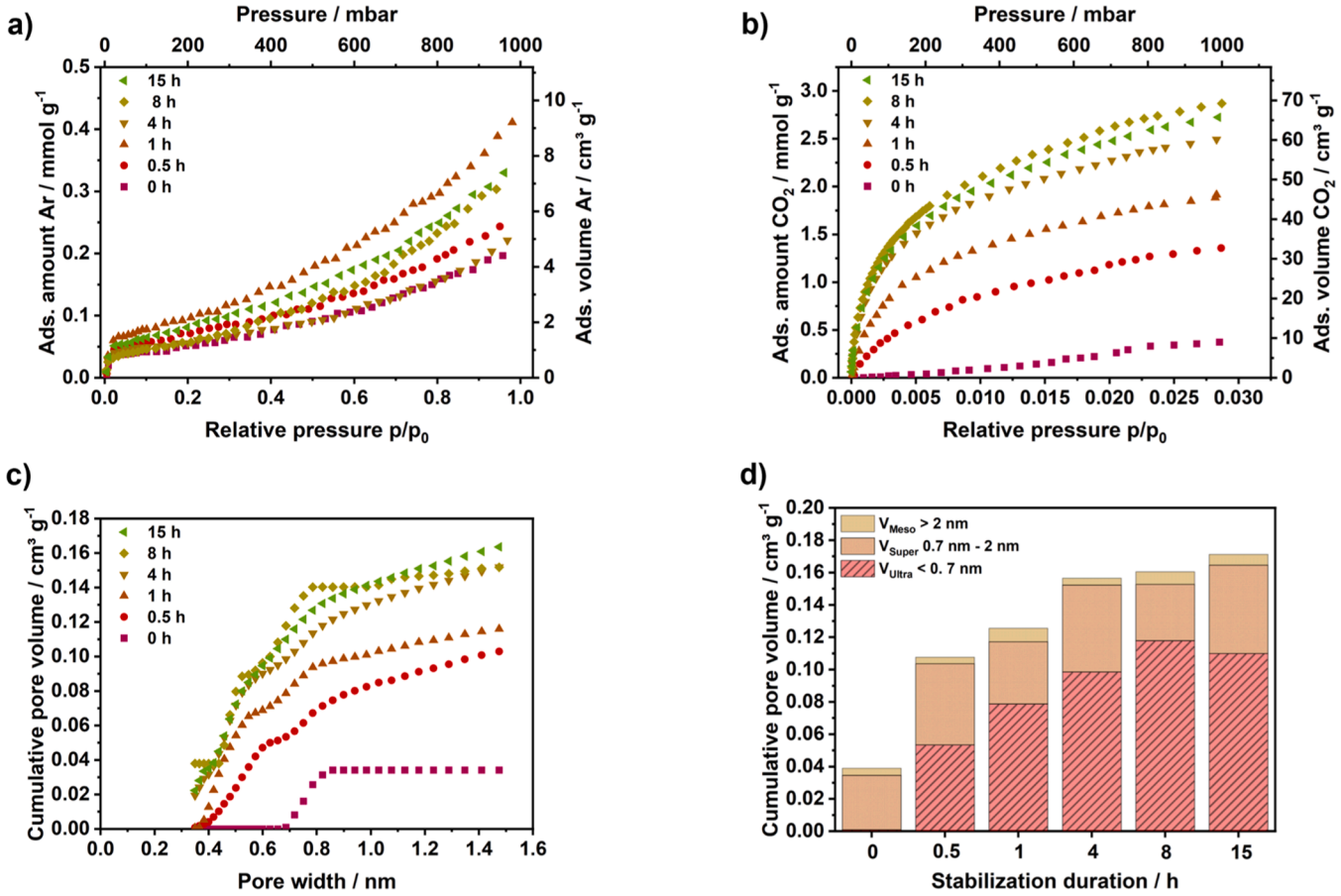

Fig. 5. (a) Ar adsorption isotherms measured at 87 K on carbon nanofibers stabilized at durations of 0–15 h. (b) CO_2 adsorption isotherms measured at 273 K for carbon nanofiber stabilized at 0–15 h duration. (c) Cumulative pore size distribution for carbon nanofibers stabilized for durations of 0–15 h at 250 °C in air. (d) Cumulative pore volume separated into ultramicropore (< 0.7 nm), supermicropore (0.7–2 nm) and mesopore (> 2 nm) region. Results of DFT calculations based on Ar at 87 K and Monte Carlo calculations based on CO_2 isotherms at 273 K were combined. All measurements were conducted on carbonized samples.

Table 1
BET area, V_{MC}, V_{DFT}, V_{Ultra}, V_{Super} and V_{Meso} and V_{total} of carbon nanofibers, which were thermally stabilized at durations of 0, 0.5, 1, 4, 8 and 15 h at 250 °C in air. Subsequently, all samples were carbonized for 3 h in Ar at 800 °C.

DURATION *[h]*	BET AREA *[$m^2\ g^{-1}$]*	V_{MC} *[$cm^3\ g^{-1}$]*	V_{DFT} *[$cm^3\ g^{-1}$]*	V_{ULTRA} *[$cm^3\ g^{-1}$]*	V_{SUPER} *[$cm^3\ g^{-1}$]*	V_{MESO} *[$cm^3\ g^{-1}$]*	V_{TOTAL} *[$cm^3\ g^{-1}$]*
0	3.2	0.034	0.005	$9.5 * 10^{-4}$	0.034	0.004	0.039
0.5	4.7	0.103	0.006	0.053	0.050	0.004	0.108
1	6.7	0.116	0.011	0.079	0.038	0.008	0.126
4	3.9	0.152	0.006	0.098	0.054	0.004	0.157
8	4.4	0.152	0.009	0.118	0.035	0.008	0.160
15	5.9	0.164	0.009	0.110	0.055	0.007	0.171

pressure region (< 0.01) rises and the adsorption capacity at 1 bar increases to 1.36 (0.5 h) and 1.88 mmol g^{-1} (1 h). For stabilization durations exceeding 4 h, this trend continues and the adsorption isotherms turn into a type I shape. Such isotherm shapes are characteristic for highly microporous adsorbents. The CO_2 adsorption capacity at 1 bar approaches a limiting value of 2.86 mmol g^{-1} on carbon nanofibers stabilized for 8 and 15 h.

Based on the CO_2 adsorption isotherms, the pore size distribution was determined using Monte-Carlo calculations with a kernel for slit pores on carbon (Fig. 5c, Table 1). On carbon nanofibers without thermal stabilization (0 h) a negligible V_{Ultra} (< 0.7 nm) is present. Between 0.7 and 0.9 nm a steep increase of the pore volume to 0.039 $cm^3\ g^{-1}$ is visible. At larger pore widths the pore volume remains almost constant.

For longer stabilization durations V_{Ultra} (< 0.7 nm) of the carbon nanofibers significantly increases to 0.118 $cm^3\ g^{-1}$ (8 h).

Since Ar and CO_2 pore size distributions cover only particular pore width regions, both were combined to give a holistic description of the pore size distributions (Fig. 5d). V_{Ultra} is taken from Monte-Carlo calculations, whereas the supermicropore volume (V_{super}) is a combination of Monte-Carlo (CO_2) and QSDFT (Ar) calculations and the mesopore volume (V_{Meso}) is solely based on the QSDFT calculations.

As discussed previously, a distinct increase of V_{Ultra} is obtained at longer stabilization durations. However, far less changes are observed in V_{super} and V_{Meso}. The V_{super} of the non-stabilized carbon nanofibers (0 h) was at 0.034 $cm^3\ g^{-1}$ and increased to 0.055 $cm^3\ g^{-1}$ for 15 h stabilization duration. However, no clear correlation to the increasing stabilization duration is visible. V_{Meso} stays on a negligible level and varies between 0.004 $cm^3\ g^{-1}$ for 0.5 h and 0.007 $cm^3\ g^{-1}$ for 15 h stabilization without a significant influence of the duration (Table 1).

Overall, a high impact of the stabilization duration on the pore formation of the carbon nanofibers is found. Especially, the formation of V_{Ultra} highly depends on the progress of the stabilization reactions.

3.2. Impact of stabilization temperature (200–300 °C)

Similar to the variation of stabilization duration, the stabilization temperature was varied between 200, 225, 250, 275 and 300 °C while keeping the duration constant at 1 h. After stabilization, the nanofibers underwent a color change from white to brownish as already observed for the variation of stabilization duration (Figure S2b).

3.2.1. Characterization

The chemical changes of the PAN structure depending on the stabilization temperature were investigated by FT-IR spectroscopy (Fig. 6a, b). To ensure comparability, all spectra were normalized to the peak height of the nitrile valence vibration ($\nu_{C\equiv N}$) of the non-stabilized samples. The non-normalized spectra are attached in Figure S3b and give an improved visualization of the individual absorption bands.

The sample stabilized at 200 °C shows a sharp signal at 2243 cm^{-1} which is assigned to $\nu_{C\equiv N}$. Additionally, the ν_{CH2} and δ_{CH2} vibrations of the polymer backbone are visible at 2930 cm^{-1}, respectively 1454 cm^{-1}. At increased stabilization temperatures the intensity of $\nu_{C\equiv N}$ decreases and the δ_{CH2} vibrations are increasingly overlapped by several absorption bands in the region of 1700–1000 cm^{-1}. As already discussed in the chapter on the stabilization duration, these arise from δ_{CH} vibrations of the cyclized structures as well as absorption bands related to oxygen containing functional surface groups, e.g. carbonyl and carboxyl.

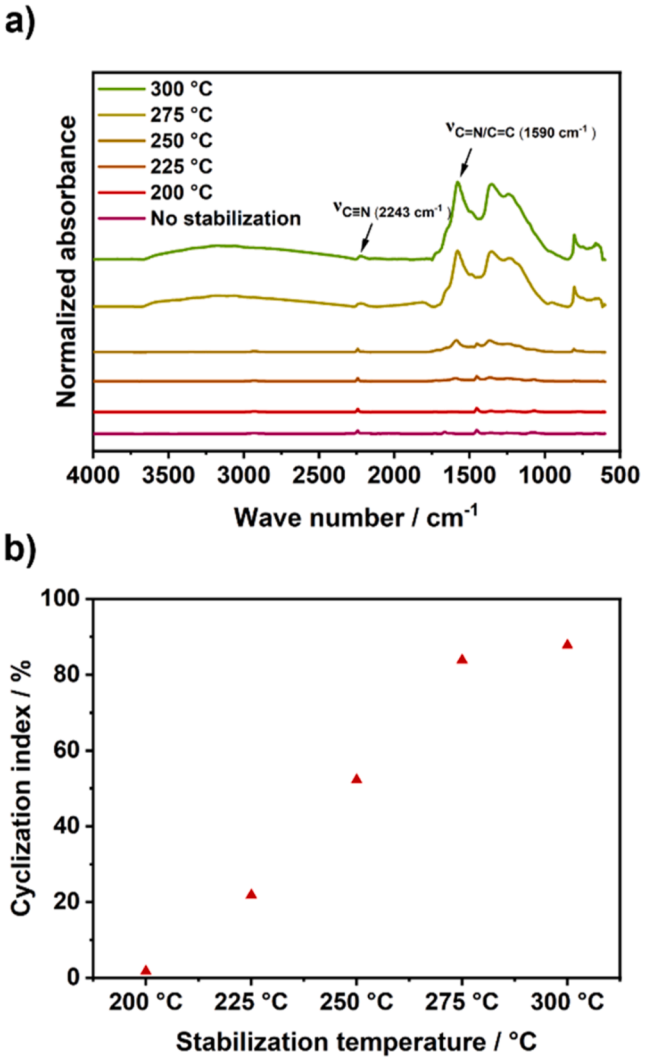

Fig. 6. (a) IR spectra of thermally stabilized PAN nanofibers. The stabilization temperature was set to 200, 225, 250, 275 and 300 °C. (b) The cyclization index determined using Eq. (1) to assess the progress of stabilization.

Additionally, a narrow absorption band at 801 cm^{-1}, reflecting the out-of-plane vibrations of the aromatic-H, is visible on samples stabilized at temperatures higher than 250 °C.

Moreover, a broad absorption band between wave numbers of 2200–3700 cm^{-1} is observed prior to carbonization. This is assigned to ν_{O-H} of adsorbed water attracted by an increased number of polar surface groups due to oxygen incorporation. This increased water adsorption was confirmed for the samples at long stabilization durations

(Figure S4).

As measure of the stabilization progress, the cyclization index was calculated (Eq. (1), Fig. 6b). At 200 °C, a low cyclization index of just 2.6 % was determined. At higher stabilization temperatures, this index increases steadily and reaches a value of 53.3 % at a stabilization temperature of 250 °C. Afterwards, it approaches a maximum of 85–87 % at stabilization temperatures of 275 and 300 °C. The cyclization indices agree well to the qualitative discussion of the IR spectra and clearly show the distinct impact of the stabilization temperature on the formation of the stabilized ladder polymer.

To determine changes in the elemental composition, the C, H, N and O fractions of the stabilized nanofibers and the carbon nanofibers were analyzed (Fig. 7a,b,c). The carbon fraction of the stabilized nanofibers decreased with increasing stabilization temperatures from 66.1 wt.- % (200 °C) to 54.7 wt.- % (300 °C).

Simultaneously, the N fraction decreased by 5.7 wt.-% from 26.2 to 20.5 wt.-% and the H fraction from 6.0 to 3.0 wt.-%. Contrarily, a significant increase of the oxygen fraction from 1.9 to 21.5 wt.-% was observed. This significant increase of the oxygen fraction is caused by the incorporation of oxygen into the stabilized ladder polymer resulting in the formation of carbonyl moieties**.** The existence of these functional groups was confirmed in ^{13}C MAS-NMR experiments (see below). The high oxygen incorporation causes the relative decrease of the C, N and H fractions. Additionally, the decrease of the H fraction is caused by the dehydrogenation reactions during stabilization. Comparing the influence of stabilization temperature and duration on the elemental composition, similar effects were observed for longer duration as well as higher temperatures. This indicates comparable impacts of duration and temperature on the stabilization reactions.

After carbonization, the C fraction of the carbon nanofibers stabilized at different temperatures lies between 70.9 and 74.7 wt.-%, decreasing slightly at higher stabilization temperatures. The N and H fractions remain almost constant between 14.1 to 16.3 wt.-%, respectively 1.2 to 1.6 wt.-%. In contrast, the O fraction increases for higher stabilization temperatures from 7.3 to 15.0 wt.-%.

Compared to the elemental composition after stabilization a 10 to 15 wt.-% increase of the carbon fraction is obtained on the carbonized samples. This increase and the simultaneous decrease of the heteroatom content was expected due to the reactions during carbonization which involve the removal of heteroatoms. Thus, the high amount of oxygen, which was incorporated during stabilization at temperatures > 250 °C, almost vanished after carbonization. This can be assigned to a high number of crosslinking condensation reactions between the stabilized ladder polymers. The high removal of oxygen during carbonization is reflected in a distinct decrease of the oxygen:carbon ratio (Fig. 7c). On samples stabilized at temperatures lower than 250 °C, the nanofibers contain only small fractions of oxygen, thus the oxygen removal is surpassed by carbon removal during carbonization. This explains the increased oxygen:carbon ratio after carbonization.

Previously discussed FT-IR and elemental analysis results indicated a high oxygen incorporation during stabilization at extended stabilization conditions. However, these results did not provide information on the oxygen bonds in the stabilized ladder structure, thus ^{13}C MAS NMR measurements were performed on two samples (1 h, 200 °C and 15 h, 250 °C) (Fig. 8).

The spectrum of the sample stabilized at 1 h, 200 °C exhibits two distinct peaks (Fig. 8a) at 28.5 and 121.7 ppm. The first is assigned to aliphatic carbon atoms (C^1, C^2) and the latter originates from the carbon atom bond to the nitrogen atom (C^3). Overall, the spectrum matches the literature spectrum of non-stabilized PAN well [48–51], which is in line with the expected low degree of stabilization.

In contrast, a significant change of the spectrum is obvious for the highly stabilized sample (15 h, 250 °C) (Fig. 8b,d). The aliphatic peak ($C^{2,aliph.}$) at 28.2 ppm almost vanished, which confirms a high degree of cyclization during thermal stabilization. The remaining signal is related to non-cyclized and aliphatic structures, which are additionally

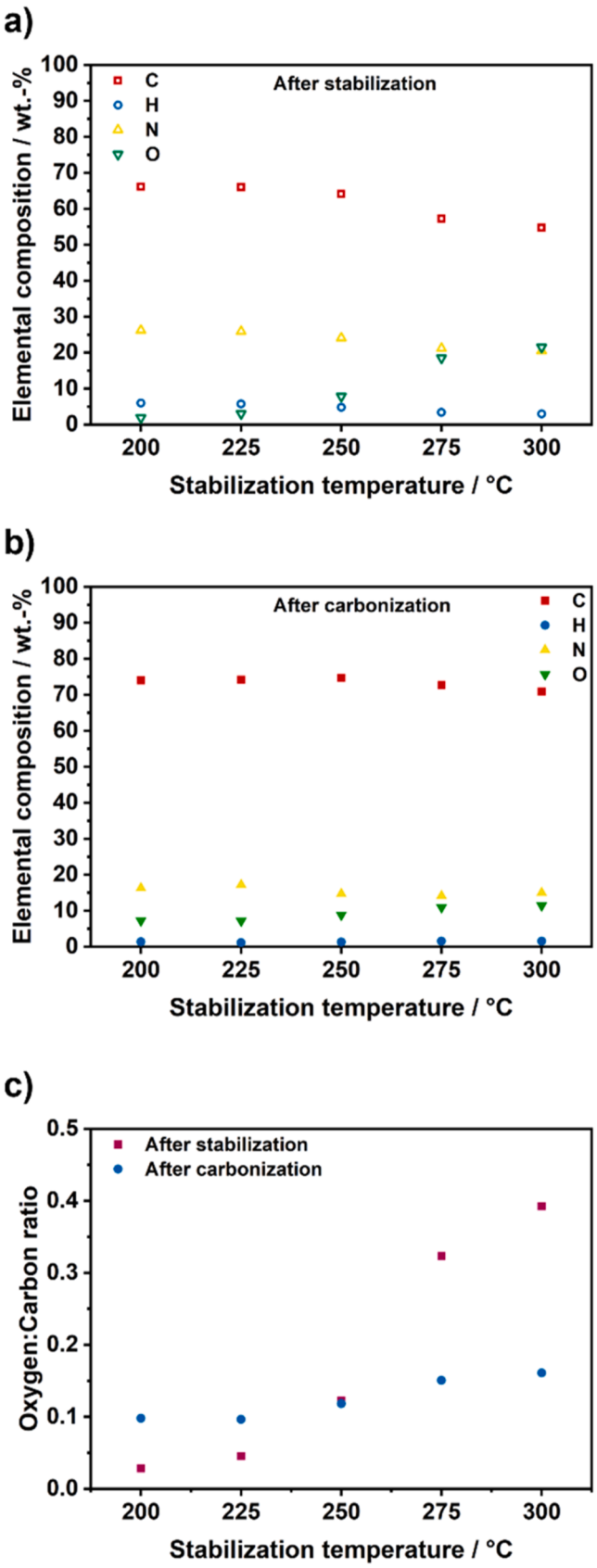

Fig. 7. (a) C, H, N, O elemental analysis of stabilized nanofibers treated at 200, 225, 250, 275 and 300 °C in air for 1 h. (b) C, H, N, O elemental analysis of carbonized nanofibers made from the stabilized nanofibers shown in (a). All carbonizations were conducted at 800 °C in Ar for 3 h. (c) Oxygen:carbon ratio for the nanofibers after stabilization and after carbonization.

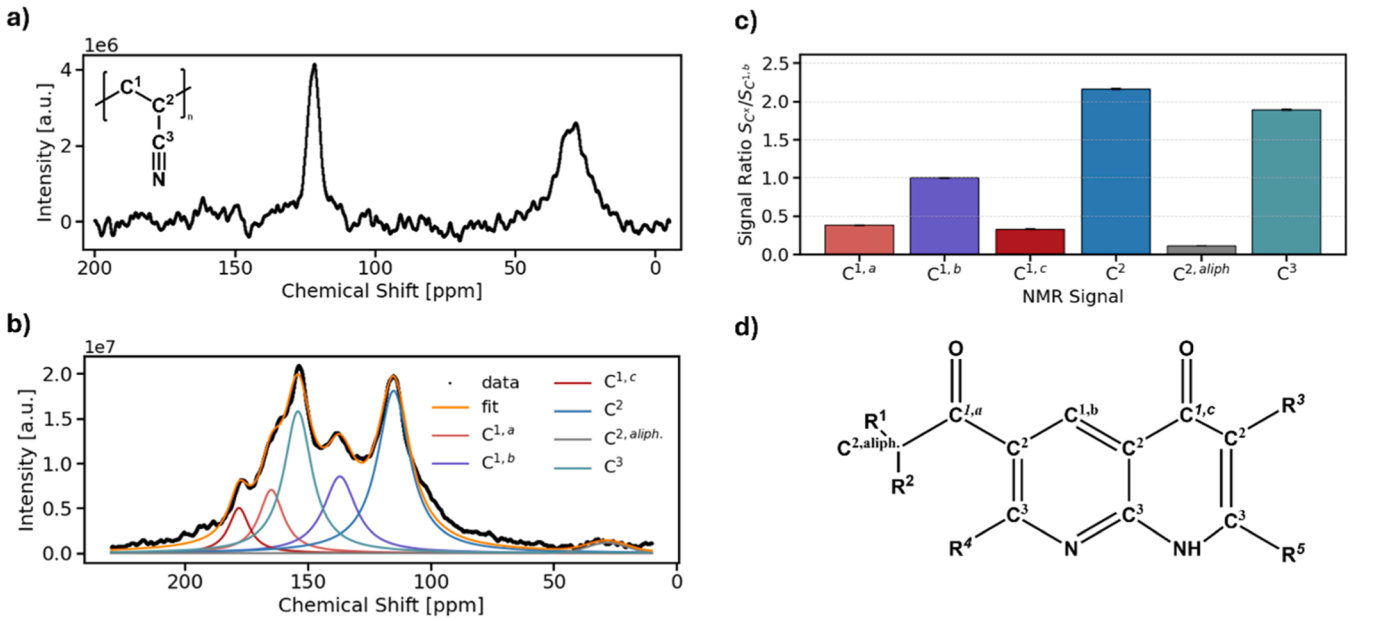

Fig. 8. (a) Solid state ^{13}C NMR spectrum of thermally stabilized nanofibers treated for 1 h at 200 °C in air and (b) treated for 15 h at 250 °C in air. (c) Signal ratio of the different carbon peaks shown in (b) to $C^{1,b}$. (d) Assignment of the different carbon peaks to the thermally stabilized ladder structure.

superimposed by the spinning side band of aromatic signals [52]. Thus, the degree of residual aliphatic structures is even lower than depicted in the spectrum.

New components arose between 75 and 200 ppm. A deconvolution of the spectrum was conducted assuming the formation of heterocyclic aromatic rings as postulated for thermal stabilization (Fig. 1). Three fits at 115.1, 136.9 and 154.5 ppm represent the three different carbon environments of the idealized heteroaromatic structure ($C^{1,b}$, C^2, C^3) which agrees well to previously published results as well as to the features of the ^{13}C spectrum of pyridine [51,53].

Additionally, two components were found between 160 to180 ppm that were attributed to carbonylic carbon atoms ($C^{1,a}$, $C^{1,c}$) due to their chemical shift (Fig. 8b,d). The formation of these carbonyl moieties is assigned to oxygen incorporation during thermal stabilization.

A clear assignment of the two carbonyl carbons at 164.9 and 177.6 ppm to a specific functional group is not feasible based on the experimental data, but it can be confined to ketone, aldehyde or carbonic acid moieties.

Earlier works assigned a signal at 175 ppm to a carbonyl bond within the aromatic system [51], which suits to the 177.6 ppm peak. The second might be attributed to a carbonyl group bond to an aliphatic segment of the ladder polymer. The formation of these carbonyl bonds is assigned to oxygen incorporation during thermal stabilization.

In Fig. 8c the different carbon moieties are quantified normalized to the $C^{1,b}$ carbon. The ratio of carbonyl moieties $C^{1,a}$ and $C^{1,c}$ to $C^{1,b}$ is 0.38 and 0.33, which results in a 0.71:1 ratio of $C^{1,a} + C^{1,c}$ to $C^{1,b}$. Therefore, approximately 40 % of the C^1 atoms, or roughly every second heteroaromatic ring, bear carbonyl moieties after thermal stabilization for 15 h at 250 °C in air.

For the underlying structural unit of polyacrylonitrile a carbon atom ratio C^1:C^2:C^3 of 1:1:1 is expected based on the proposed structure (Fig. 8d). Determining the C^1:C^2:C^3 ratio based on the experimental data, summing up $C^{1,a}$, $C^{1,b}$ and $C^{1,c}$ to C^1, a ratio of 1.71:1.89:2.17 is obtained. This matches the expected 1:1:1 ratio quite well considering possible structural deviations, e.g. incomplete cyclization and non-aromatic segments.

In total, the ^{13}C MAS NMR results confirm the incorporation of oxygen as carbonyl moiety into the stabilized ladder structure. This supports the previous results and the hypothesis that the carbonyl groups could enable additional crosslinking reactions via condensation of carbonyl groups during subsequent carbonization.

The larger stabilized ladder polymers and the proposed higher number of condensation reactions between the stabilized ladder polymers during carbonization due to a higher number of carbonyl functional groups might result in the formation of larger carbon frameworks, as observed for the samples stabilized for different durations (see Section 3.1.1).

Therefore, Raman spectroscopy was used to assess the degree of structural order by evaluation of the D_1/G ratio. In Fig. 9a the characteristic D and G band region of the Raman spectrum of the carbon nanofibers is depicted. Similar to the discussion in Section 3.1.1 five Gaussian fits, D_1, D_2, D_3, D_4 and G are used for deconvolution and by integration of the D_1 and the G peak area, the D_1/G ratio was determined (S7). In Fig. 9b a decrease of the D_1/G ratio from 1.71 to 1.51 at increasing stabilization temperature is visible. This is assigned to an increased structural order of the carbon network of carbon nanofibers stabilized at higher temperatures.

As the carbonization conditions were kept constant for all samples, the differences in the structural order are related to the stabilization process, respectively the stabilization temperature. The increased structural order can be attributed to the formation of larger stabilized ladder polymers at higher stabilization temperatures, indicated by the increased cyclization index, and the formation of carbonyl surface groups during stabilization (see NMR results) which allow for additional crosslinking reactions between the stabilized ladder polymers during carbonization via condensation reactions.

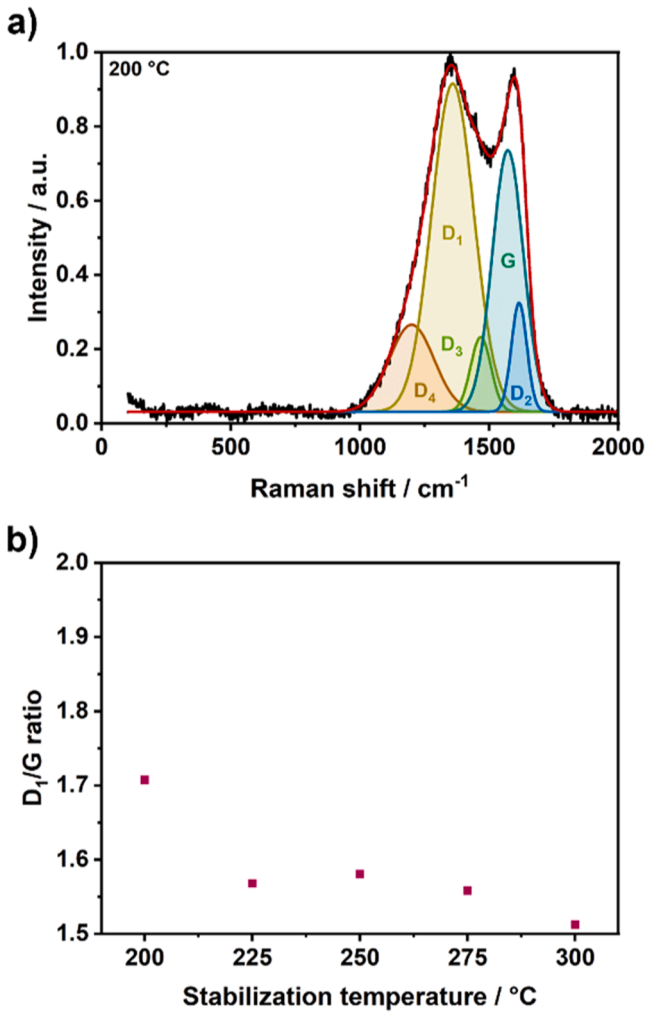

Fig. 9. (a) Raman spectrum of the D and G band region for carbon nanofibers stabilized at 200 °C for 1 h in air. The spectrum was measured after carbonization at 800 °C for 3 h in Ar. (b) D_1/G ratio was determined based on integration of the D and G band region for carbon nanofibers stabilized at 200, 225, 250, 275 and 300 °C for 1 h.

3.2.2. *Impact on the pore structure*

As conducted for the stabilization duration series, the pore structure development of the temperature series was investigated by means of Ar and CO_2 gas adsorption measurements.

In the Ar adsorption measurements, all samples showed type II isotherms with capacities <0.5 mmol g^{-1} at 1 bar (Fig. 10a). Within the sample series, no trends with respect to the stabilization temperature were observed. Based on the Ar isotherms, the BET area was determined, which was below 7 m^2 g^{-1} for all samples (Table 2). Additionally, the pore size distribution was calculated based on a QSDFT model for slit pores on carbon. Negligible cumulative pore volumes of up to 0.011 cm^3 g^{-1} were determined (Table 2, Figure S6b). Overall, the shape of the isotherm, the low Ar capacities, the small BET area and the negligible cumulative pore volume are typical for a non-porous adsorbent or an adsorbent with pores not accessible for the adsorptive.

Since narrow micropores are inaccessible for Ar due to its critical diameter, CO_2 isotherms at 273 K were measured to assess the present micro- and ultramicropore volume (Fig. 10b). An almost linear adsorption isotherm is obtained on the 200 °C sample with a low CO_2 uptake of 0.3 mmol g^{-1} at 1 bar. At higher stabilization temperatures, the CO_2 capacity and the isotherm slope in the low-pressure region (p/p_0 < 0.01) increase distinctly. For samples stabilized at temperatures >250 °C, the isotherm turns into a type I shape which is characteristic for highly microporous adsorbents. The CO_2 adsorption capacity at 1 bar rises to 2.7 mmol g^{-1} on these samples.

The CO_2 adsorption isotherms were used to determine the pore size distribution based on Monte-Carlo calculations with a kernel for slit pores on carbon (Fig. 10c). The sample stabilized at 200 °C contains only pores larger than 0.6 nm and reaches a cumulative pore volume (V_{MC}) of 0.027 cm^3 g^{-1}. These values are comparable to the pore volume of carbon nanofibers without thermal stabilization (Table 1, 0 h). At increasing stabilization temperature, V_{MC} rises steadily and results in a maximum of 0.16 cm^3 g^{-1} on samples stabilized at 275 and 300 °C. Within V_{MC}, a significant increase of the V_{Ultra} (<0.7 nm) is observed. Especially this high formation of V_{Ultra} results in the distinct increase of the CO_2 adsorption capacities.

The cumulative pore size distributions obtained from the Ar and CO_2 isotherms were combined to give a holistic overview on the pore size distribution of the samples (Fig. 9d). To do so, the gained data was separated into three pore regions: Ultramicropore volume $V_{Ultra\ (<0.7\ nm)}$, supermicropore volume $V_{Super\ (0.7–2\ nm)}$ and mesopore volume $V_{Meso\ (>2\ nm)}$. V_{Super} is made up of V_{MC} in the range of 0.7–1.5 nm and V_{DFT} in the range from 1.5–2 nm. The others are based solely on the respective applicable method. The present V_{Ultra} rises from 0.007 cm^3 g^{-1} (200 °C) to 0.112 cm^3 g^{-1} (300 °C). In contrast, V_{super} varies between 0.034 cm^3 g^{-1} to 0.048 cm^3 g^{-1} without a clear trend and V_{Meso} stays on a negligible level between 0.004 to 0.008 cm^3 g^{-1}. This clearly points out the distinct effect of stabilization temperature on the formation of the ultramicropore volume. Overall, the impact is comparable to the impact observed for the stabilization duration

3.3. *Correlating changes during stabilization and pore structure*

The previously discussed results showed significant impacts of the stabilization conditions on the stabilization progress. Additionally, gas adsorption measurements on carbonized samples revealed distinct effects on the pore formation and the adsorption capacities. This section targets on correlating both results.

In Fig. 11a, the correlation of the oxygen content to the cyclization index is depicted. Both increase at more intense stabilization treatment (higher temperature, longer duration) as the reactions are promoted by the supplied additional energy. Since both, the oxygen content and the cyclization index, are strongly influenced by the intensity of stabilization conditions, a causal relationship is rather unlikely. Nonetheless, the good agreement between the duration and temperature series confirms the similar impact of duration and temperature variation on the stabilization process.

Furthermore, a good correlation of V_{Ultra} to the increasing cyclization index was found (Fig. 11b).

At higher cyclization indices, V_{Ultra} of the carbonized nanofibers increases steadily. The variation of stabilization duration and temperature have very similar effects. Similarly, good correlations of V_{Ultra} to the oxygen content after stabilization were obtained (Fig. 11c). A steep increase of V_{Ultra} is visible for low oxygen contents which approaches a

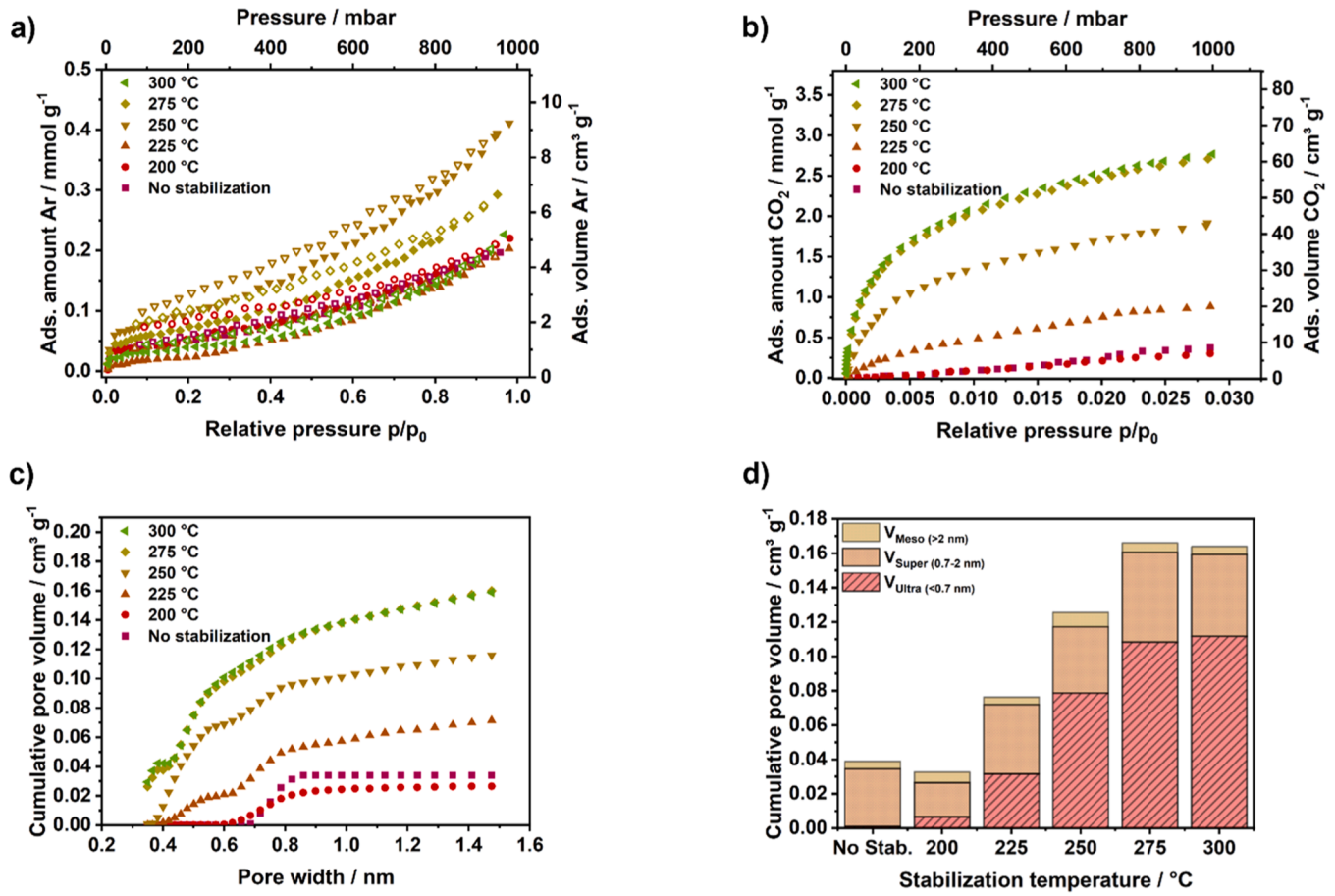

Fig. 10. (a) Ar adsorption isotherms measured at 87 K and (b) CO_2 adsorption isotherms measured at 273 K on carbon nanofiber stabilized at 200, 225, 250, 275 and 300 °C for 1 h in air. (c) Cumulative pore size distribution for carbon nanofibers stabilized at temperatures of 200–300 °C for 1 h in air. The cumulative pore volume was obtained by Monte-Carlo calculations using a model for slit pores on carbon. (d) Cumulative pore volume divided into ultramicropore (< 0.7 nm), supermicropore (0.7–2 nm) and mesopore (> 2 nm) region. Results of DFT calculations based on Ar at 87 K and Monte Carlo calculations based on CO_2 isotherms at 273 K were combined in this figure. All measurements were conducted on carbonized samples (800 °C, 3 h, Ar).

Table 2
BET area, V_{MC}, V_{DFT}, V_{Ultra}, V_{Super} and V_{Meso} and V_{total} of carbon nanofibers, which were thermally stabilized at temperatures of 200, 225, 250, 275 and 300 °C for 1 h in air. Subsequently, all samples were carbonized for 3 h in Ar at 800 °C.

TEMPERATURE [°C]	BET AREA [$m^2\ g^{-1}$]	V_{DFT} [$cm^3\ g^{-1}$]	V_{MC} [$cm^3\ g^{-1}$]	V_{ULTRA} [$cm^3\ g^{-1}$]	V_{SUPER} [$cm^3\ g^{-1}$]	V_{MESO} [$cm^3\ g^{-1}$]	V_{TOTAL} [$cm^3\ g^{-1}$]
200	3.5	0.006	0.027	0.007	0.020	0.006	0.032
225	1.8	0.005	0.071	0.032	0.040	0.004	0.076
250	6.7	0.011	0.12	0.079	0.038	0.008	0.126
275	5.1	0.008	0.16	0.108	0.052	0.006	0.166
300	3.1	0.006	0.16	0.112	0.048	0.005	0.164

limiting value for oxygen contents of 20–25 wt.- %.

The correlation of V_{Ultra} to these parameters, cyclization index and oxygen content, shows a plausible causal relationship. The formation of V_{Ultra} occurs during carbonization, whereas oxygen incorporation and cyclization take place during stabilization. Thus, V_{Ultra} formation and oxygen incorporation and cyclization cannot be affected by identical parameters. However, the correlations of V_{Ultra} to the oxygen content and the cyclization index show that the increase of V_{Ultra} during carbonization is likely to be dependent on these parameters. Nonetheless, it is conceivable that V_{Ultra} is affected by further parameters which were not considered here.

In total, the discussed correlations imply that V_{Ultra} formation during carbonization depends on the oxygen incorporation and the cyclization progress during stabilization. Both are adjustable by variation of the

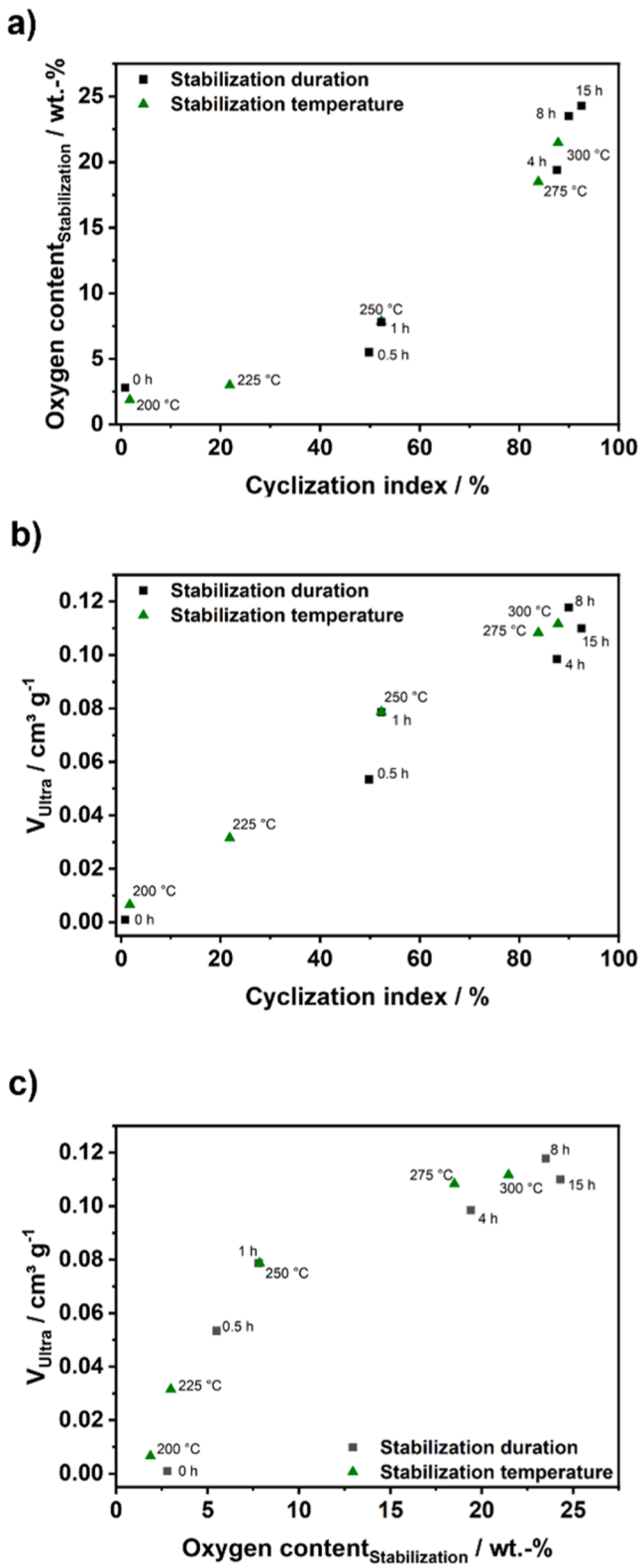

Fig. 11. Correlation of a) the oxygen content and cyclization index determined after stabilization, b) V_{Ultra} to the cyclization index and c) V_{Ultra} to oxygen content after stabilization. V_{Ultra} was determined after carbonization. The samples were synthesized at different stabilization duration from 0–15 h at 250 °C and at different temperatures from 200 to 300 °C for 1 h. All stabilization were conducted in air. The carbonization was conducted at 800 °C in Ar for 3 h.

stabilization duration or the stabilization temperature. Thus, the thermal stabilization conditions need careful consideration for tailoring the pore volume of PAN-based carbon nanofibers.

4. Conclusion

The impact of the stabilization duration (0–15 h) and the stabilization temperature (200–300 °C) on the pore formation of electrospun carbon nanofibers was investigated. All pore size analysis was conducted on carbon nanofibers.

A significant impact of the stabilization duration on the pore formation during carbonization was found. Non-stabilized carbon nanofibers showed a low total cumulative pore volume (V_{total}) of 0.039 $cm^3\ g^{-1}$. Moreover, their ultramicropore volume (V_{Ultra}) was on a negligible level. At elevating the stabilization duration, the V_{total} increased steadily to a maximum of 0.171 $cm^3\ g^{-1}$ after 15 h. Especially worth mentioning is the significant rise of V_{Ultra} to 0.118 $cm^3\ g^{-1}$. This increase in V_{ultra} is also reflected in a change of the linear adsorption isotherm into a type I shape for durations $\geq$ 4 h.

Similar results were obtained by variation of the stabilization temperature. A temperature increase from 200 °C to 300 °C resulted in a growth of V_{total} from 0.032 to 0.166 $cm^3\ g^{-1}$ on the carbonized nanofibers. Likewise, a distinct increase in V_{Ultra} from 0.007 to 0.112 $cm^3\ g^{-1}$ was determined, which resulted in a type I shaped isotherm for samples stabilized at temperatures $\geq$ 275 °C.

The supplementing analyses on the stabilization process showed a distinct effect of stabilization duration and temperature on the growth of the stabilized ladder polymer and the incorporation of oxygen into the structure. The latter was confirmed in NMR measurements showing the formation of carbonyl moieties at intense stabilization conditions. Linking these results to the gas adsorption measurements, the two factors, oxygen content and cyclization degree, are seen as essential parameters which govern the formation of the pore volume during carbonization. In particular, the formation of V_{Ultra} appears to be significantly dependent on these factors. Overall, the gained results clearly demonstrate the need to consider the stabilization conditions for tailoring the pore volume of carbon nanofibers.

CRediT authorship contribution statement

T. Fischer: Writing – original draft, Visualization, Methodology, Investigation, Conceptualization. **M. Pagel:** Writing – review & editing, Methodology, Investigation. **A. Kretzschmar:** Writing – review & editing, Supervision, Methodology, Conceptualization. **V. Selmert:** Writing – review & editing, Methodology, Conceptualization. **S. Jovanovic:** Writing – review & editing, Methodology, Investigation. **R. Rameker:** Writing – review & editing, Methodology, Investigation. **H. Kungl:** Writing – review & editing, Conceptualization. **H. Tempel:** Writing – review & editing, Supervision, Project administration, Funding acquisition. **R.-A. Eichel:** Supervision, Project administration, Funding acquisition, Conceptualization.

Declaration of competing interest

The authors declare that they have no known competing financial interests or personal relationships that could have appeared to influence the work reported in this paper.

Acknowledgements

The authors acknowledge funding provided by the Deutsche Forschungsgemeinschaft (DFG, German Research Foundation) under Germany's Excellence Strategy-Cluster of Excellence 2186 'The Fuel Science Center' ID:390919832.

Supplementary materials

Supplementary material associated with this article can be found, in the online version, at doi:10.1016/j.cartre.2025.100559.

Data availability

Data will be made available on request.

References

[1] E. Fitzer, PAN-based carbon fibers-present state and trend of the technology from the viewpoint of possibilities and limits to influence and to control the fiber properties by the process parameters, Carbon. N. Y 27 (5) (1989) 621–645, https://doi.org/10.1016/0008-6223(89)90197-8.

[2] R. Soni, R. Verma, R. Kumar Garg, V. Sharma, A critical review of recent advances in the aerospace materials, Mater. Today:. Proc. (113) (2023) 180–184, https://doi.org/10.1016/j.matpr.2023.08.108.

[3] R. Soni, R. Verma, R. Kumar Garg, H. Singh, Progress in aerospace materials and ablation resistant coatings: a focused review, Opt. Laser. Technol. 177 (2024) 1–18, https://doi.org/10.1016/j.optlastec.2024.111160.

[4] K. Li, X. Ni, Q. Wu, C. Yuan, C. Li, et al., Carbon-based fibers: fabrication, characterization and application, Adv. Fiber. Mater 4 (4) (2022) 631–682, https://doi.org/10.1007/s42765-022-00134-x.

[5] H. Ahmad, A.A. Markina, M.V. Porotnikov, F. Ahmad, A review of carbon fiber materials in automotive industry, IOP. Conf. Ser.: Mater. Sci. Eng 971 (2020) 1–9, https://doi.org/10.1088/1757-899X/971/3/032011.

[6] J. Zhang, G. Lin, U. Vaidya, H. Wang, Past, present and future prospective of global carbon fibre composite developments and applications, Compos. B:. Eng. 250 (2023) 1–19, https://doi.org/10.1016/j.compositesb.2022.110463.

[7] A.G. Pandolfo, A.F. Hollenkamp, Carbon properties and their role in supercapacitors, J. Power. Sources 157 (1) (2006) 11–27, https://doi.org/10.1016/j.jpowsour.2006.02.065.

[8] X.-Y. Li, Y. Yan, B. Zhang, T.-J. Bai, Z.-Z. Wang, et al., PAN-derived electrospun nanofibers for supercapacitor applications: ongoing approaches and challenges, J. Mater. Sci 56 (18) (2021) 10745–10781, https://doi.org/10.1007/s10853-021-05939-6.

[9] T. Fischer, A. Kretzschmar, V. Selmert, S. Jovanovic, H. Kungl, et al., Post-treatment strategies for pyrophoric KOH-activated carbon nanofibres, RSC. Adv 14 (6) (2024) 3845–3856, https://doi.org/10.1039/d3ra07096d.

[10] V. Selmert, A. Kretzschmar, H. Weinrich, H. Kungl, H. Tempel, et al., CO_2/N_2 separation on highly selective carbon nanofibers investigated by dynamic gas adsorption, ChemSusChem 15 (2022) 1–12, https://doi.org/10.1002/cssc.202200761.

[11] V. Selmert, A. Kretzschmar, H. Kungl, H. Tempel, R.-A. Eichel, Breakthrough analysis of the CO2/CH4 separation on electrospun carbon nanofibers, Adsorption 30 (1) (2024) 107–119, https://doi.org/10.1007/s10450-023-00435-6.

[12] Y.-J. Heo, Y. Zhang, K.Y. Rhee, S.-J. Park, Synthesis of PAN/PVDF nanofiber composites-based carbon adsorbents for CO2 capture, Compos. B:. Eng. 156 (2019) 95–99, https://doi.org/10.1016/j.compositesb.2018.08.057.

[13] P.J. Goodhew, A.J. Clarke, J.E. Bailey, A review of the farbication and properties of carbon fibers, Mater. Sci. Eng. 17 (1975) 3–30.

[14] M.S.A. Rahaman, A.F. Ismail, A. Mustafa, A review of heat treatment on polyacrylonitrile fiber, Polym. Degrad. Stab 92 (8) (2007) 1421–1432, https://doi.org/10.1016/j.polymdegradstab.2007.03.023.

[15] E. Frank, F. Hermanutz, M.R. Buchmeiser, Carbon fibers: precursors, manufacturing, and properties, Macromol. Mater. Eng 297 (6) (2012) 493–501, https://doi.org/10.1002/mame.201100406.

[16] E. Fitzer, D.J. Müller, The influence of oxygen on the chemical reactions during stabilization of PAN as carbon fiber precursor, Carbon. N. Y 13 (1975) 63–69, https://doi.org/10.1016/0008-6223(75)90259-6.

[17] E. Fitzer, W. Frohs, M. Heine, Optimization of stabilization and carbonization treatment of PAN fibres and structural characterization of the resulting carbon fibres, Carbon. N. Y 24 (1986) 387–395, https://doi.org/10.1016/0008-6223(86)90257-5.

[18] J. Liu, P.H. Wang, R.Y. Li, Continuous carbonization of polyacrylonitrile-based oxidized fibers: aspects on mechanical properties and morphological structure, J. Appl. Polym. Sci 52 (7) (1994) 945–950, https://doi.org/10.1002/app.1994.070520712.

[19] H. Khayyam, R.N. Jazar, S. Nunna, G. Golkarnarenji, K. Badii, et al., PAN precursor fabrication, applications and thermal stabilization process in carbon fiber production: experimental and mathematical modelling, Prog. Mater. Sci 107 (2020) 1–39, https://doi.org/10.1016/j.pmatsci.2019.100575.

[20] S. Xiao, W. Cao, B. Wang, L. Xu, B. Chen, Mechanism and kinetics of oxidation during the thermal stabilization of polyacrylonitrile fibers, J. Appl. Polym. Sci 127 (4) (2012) 3198–3203, https://doi.org/10.1002/app.37733.

[21] T. Takahagi, I. Shimada, M. Fukuhara, K. Morita, A. Ishitani, XPS studies on the chemical structure of the stabilized polyacrylonitrile fiber in the carbon fiber production process, J. Polym. Sci. A:. Polym. Chem. 24 (1986) 3101–3107, https://doi.org/10.1002/pola.1986.080241134.

[22] R. Ojeda-López, E. Aguilar-Huerta, D.A. Maia, D.C. Azevedo, C. Felipe, et al., Tailoring synthesis conditions of carbon microfibers to enhance the microporosity, CO2 and CH4 adsorption by using the response surface methodology, Microporous. Mesoporous. Mater. 305 (2020) 1–9, https://doi.org/10.1016/j.micromeso.2020.110333.

[23] A. Kretzschmar, V. Selmert, H. Weinrich, H. Kungl, H. Tempel, et al., Tailored gas adsorption properties of electrospun carbon nanofibers for gas separation and storage, ChemSusChem 13 (12) (2020) 3180–3191, https://doi.org/10.1002/cssc.202000520.

[24] A. Kretzschmar, V. Selmert, H. Kungl, H. Tempel, R.A. Eichel, Application of a tailorable carbon molecular sieve to evaluate concepts for the molecular dimensions of gases, Microporous. Mesoporous. Mater. 343 (2022) 1–9, https://doi.org/10.1016/j.micromeso.2022.112156.

[25] Y.C. Chiang, C.-C. Huang, W.-T. Chin, Carbon dioxide adsorption on Carbon nanofibers with different porous structures, Appl. Sci. 11 (2021) 1–15, https://doi.org/10.3390/app11167724.

[26] D.-K. Kim, S.H. Park, B.C. Kim, Electrospun polyacrylonitrile-based carbon nanofibers and their hydrogen storages, Macromol. Res 13 (6) (2005) 521–528, https://doi.org/10.1007/BF03218490.

[27] E. Maruccia, S. Ferrari, M. Bartoli, L. Lucherini, G. Meligrana, et al., Effect of thermal stabilization on PAN-derived electrospun carbon nanofibers for CO(2) capture, Polym. (Basel) 13 (23) (2021) 1–13, https://doi.org/10.3390/polym13234197.

[28] R. Ojeda-López, J.M. Esparza-Schulz, I.J. Pérez-Hermosillo, A. Hernández-Gordillo, A. Domínguez-Ortiz, Improve in CO2 and CH4 adsorption capacity on carbon microfibers synthesized by electrospinning of PAN, Fibers 7 (10) (2019) 1–14, https://doi.org/10.3390/fib7100081.

[29] J. Landers, G.Y. Gor, A.V. Neimark, Density functional theory methods for characterization of porous materials, Colloids. Surf. A:. Physicochem. Eng. Asp. 437 (2013) 3–32, https://doi.org/10.1016/j.colsurfa.2013.01.007.

[30] M. Thommes, K.A. Cychosz, Physical adsorption characterization of nanoporous materials: progress and challenges, Adsorption 20 (2–3) (2014) 233–250, https://doi.org/10.1007/s10450-014-9606-z.

[31] G.L. Collins, N.W. Thomas, G.E. Williams, Kinetic relationships between heat generation and nitrile consumption in the reaction of poly(acrylonitrile) in air at 265°C, Carbon. N. Y 26 (1988) 672–679, https://doi.org/10.1016/0008-6223(88)90070-X.

[32] L. Chen, Z. Shen, J. Liu, J. Liang, X. Wang, Effects of oxygen on the structural evolution of polyacrylonitrile fibers during rapid thermal treatment, RSC. Adv 10 (11) (2020) 6356–6361, https://doi.org/10.1039/c9ra08881d.

[33] Z.E. Brubaker, J.J. Langford, R.J. Kapsimalis, J.L. Niedziela, Quantitative analysis of Raman spectral parameters for carbon fibers: practical considerations and connection to mechanical properties, J. Mater. Sci 56 (27) (2021) 15087–15121, https://doi.org/10.1007/s10853-021-06225-1.

[34] L.G. Cançado, A. Jorio, M.A. Pimenta, Measuring the absolute Raman cross section of nanographites as a function of laser energy and crystallite size, Phys. Rev. B 76 (6) (2007) 1–7, https://doi.org/10.1103/PhysRevB.76.064304.

[35] A. Cuesta, P. Dhamelincourt, J. Laureyns, A. Martinez-Alonso, J. Tascon, Raman microprobe studies on carbon materials, Carbon. N. Y 32 (8) (1994) 1523–1532.

[36] M. Newville, R. Otten, A. Nelson, T. Stensitzki, A. Ingargiola, D. Allan, A. Fox, F. Carter, M. Rawlik, LMFIT: non-linear least-squares minimization and curve-fitting for Python, Zenodo (2025).

[37] H.N. Friedlander, L.H. Peebles, J. Brandrub, J.R. Kirby, On the chromophore of polyacrylonitrile. VI. Mechanism of color formation in polyacrylonitrile, Macromolecules 1 (1) (1968) 79–86.

[38] S. Arbab, A. Teimoury, H. Mirbaha, D.C. Adolphe, B. Noroozi, et al., Optimum stabilization processing parameters for polyacrylonitrile-based carbon nanofibers and their difference with carbon (micro) fibers, Polym. Degrad. Stab 142 (2017) 198–208, https://doi.org/10.1016/j.polymdegradstab.2017.06.026.

[39] E. Cipriani, M. Zanetti, P. Bracco, V. Brunella, M.P. Luda, et al., Crosslinking and carbonization processes in PAN films and nanofibers, Polym. Degrad. Stab 123 (2016) 178–188.

[40] J. Choi, S.-S. Kim, Y.-S. Chung, S. Lee, Evolution of structural inhomogeneity in polyacrylonitrile fibers by oxidative stabilization, Carbon. N. Y 165 (2020) 225–237, https://doi.org/10.1016/j.carbon.2020.04.027.

[41] W. Watt (1985) Chemistry and physics of the conversion of polyacrylonitrile fibres into high-modulus carbon fibres, in *strong fibers* (ed W. Watt and B. Perov), pp. 327–387.

[42] Z. Li, L. Deng, I.A. Kinloch, R.J. Young, Raman spectroscopy of carbon materials and their composites: graphene, nanotubes and fibres, Prog. Mater. Sci 135 (2023) 1–58, https://doi.org/10.1016/j.pmatsci.2023.101089.

[43] A. Sadezky, H. Muckenhuber, H. Grothe, R. Niessner, U. Pöschl, Raman microspectroscopy of soot and related carbonaceous materials: spectral analysis and structural information, Carbon. N. Y 43 (8) (2005) 1731–1742, https://doi.org/10.1016/j.carbon.2005.02.018.

[44] S. Claramunt, A. Varea, D. López-Díaz, M.M. Velázquez, A. Cornet, et al., The importance of interbands on the interpretation of the Raman spectrum of graphene oxide, J. Phys. Chem. C 119 (18) (2015) 10123–10129, https://doi.org/10.1021/acs.jpcc.5b01590.

[45] C. Marino, J. Cabanero, M. Povia, C. Villevieille, Biowaste lignin-based carbonaceous materials as anodes for Na-ion batteries, J. Electrochem. Soc 165 (7) (2018) A1400–A1408, https://doi.org/10.1149/2.0681807jes.

[46] P.A. Goodman, H. Li, Y. Gao, Y.F. Lu, J.D. Stenger-Smith, et al., Preparation and characterization of high surface area, high porosity carbon monoliths from pyrolyzed bovine bone and their performance as supercapacitor electrodes, Carbon. N. Y 55 (2013) 291–298, https://doi.org/10.1016/j.carbon.2012.12.066.

[47] M. Thommes, K. Kaneko, A.V. Neimark, J.P. Olivier, F. Rodriguez-Reinoso, et al., Physisorption of gases, with special reference to the evaluation of surface area and

pore size distribution (IUPAC Technical Report), Pure. Appl. Chem. 87 (9–10) (2015) 1051–1069, https://doi.org/10.1515/pac-2014-1117.
[48] S. Xiao, B. Wang, C. Zhao, L. Xu, B. Chen, Influence of oxygen on the stabilization reaction of polyacrylonitrile fibers, J. Appl. Polym. Sci 127 (3) (2013) 2332–2338, https://doi.org/10.1002/app.37930.
[49] J. Ma, Z. Zheng, Y. Tang, H. Nagashima, T. Miyoshi, Chemical reactions in poly (acrylonitrile-co-itaconic acid) during stabilization as revealed by solid-state NMR spectroscopy and 13C isotope labeling, Carbon. N. Y 215 (2023) 118432, https://doi.org/10.1016/j.carbon.2023.118432.
[50] Y. Wang, L. Xu, M. Wang, W. Pang, X. Ge, Structural identification of polyacrylonitrile during thermal treatment by selective 13 C labeling and solid-State 13 C NMR spectroscopy, Macromolecules 47 (12) (2014) 3901–3908, https://doi.org/10.1021/ma500727n.
[51] X. Liu, W. Chen, Y. Hong, S. Yuan, S. Kuroki, et al., Stabilization of atactic -polyacrylonitrile under nitrogen and air As studied by solid-State NMR, Macromolecules 48 (15) (2015) 5300–5309, https://doi.org/10.1021/acs.macromol.5b01030.
[52] D.D. Laws, H.-M.L. Bitter, A. Jerschow, Methoden der Festkörper-NMR-Spektroskopie in der chemie, Angew. Chem. 114 (2002) 3224–3259.
[53] National Institute of Advanced Industrial Science and Technology 13C NMR pyridine, 25 July, https://sdbs.db.aist.go.jp/CompoundLanding.aspx?sdbsno=518, 2025, 25 July.